

Comparing and Combining water vapor data from GPS and MERIS.

Journal:	<i>International Journal of Remote Sensing</i>
Manuscript ID:	draft
Manuscript Type:	Special Issue Paper
Date Submitted by the Author:	n/a
Complete List of Authors:	Lindenbergh, Roderik; Delft Institute of Earth Observation and Space Systems, Section Mathematical Geodesy and Positioning Keshin, Maxim; Delft Institute of Earth Observation and Space Systems, Section Mathematical Geodesy and Positioning van der Marel, Hans; Delft Institute of Earth Observation and Space Systems, Section Mathematical Geodesy and Positioning Hanssen, Ramon; Delft Institute of Earth Observation and Space Systems, Section Mathematical Geodesy and Positioning
Keywords:	DATA ANALYSIS, GEOSTATISTICS, MERIS, METEOROLOGY
Keywords (user defined):	MERIS GPS, water vapor, spatial-temporal combination

powered by ScholarOne
Manuscript Central™

Comparing and Combining water vapor data from GPS and MERIS.

RODERIK LINDENBERGH*, MAXIM KESHIN, HANS VAN DER MAREL AND RAMON HANSSEN

Delft Institute of Earth Observation and Space Systems, Delft University of Technology,

P.O. Box 5058, 2600 GB Delft, NL

(Received 00 Month 200x; In final form 00 Month 200x)

Improved knowledge of atmospheric water vapor and its temporal and spatial variability is of great scientific interest for climate research and weather prediction, but also geodetic positioning applications using GPS and radar interferometry will benefit. In this article both a comparison and a combination is made of MERIS and GPS based integrated water vapor data, retrieved at the same day over Western Europe. For both signals a variance-covariance analysis is made, that is applied in producing a time series of combined water vapor maps by means of the geostatistical Kriging approach.

Keywords: GPS, MERIS, Kriging, water vapor, spatial-temporal

1 Introduction

Water vapor is the atmosphere's dominant greenhouse gas, (Cess, 2005; Soden et al., 2005). Besides accounting for a large part of Earth's natural greenhouse effect, gaseous water also condenses to form clouds, which act as an isolation layer for earth's surface temperature. Knowledge on water vapor values is not only essential for environmental issues but also for satellite measurements from the world wide Global Positioning System (GPS), (Bevis et al., 1992), or (Interferometric) Synthetic Aperture Radar, (In)SAR, (Hanssen, 2001). The GPS or SAR signal will be delayed by the water vapor while traveling through

*Corresponding author. Email: r.c.lindenbergh@tudelft.nl

1 the atmosphere. Unlike most other atmospheric gases, the distribution of water in the atmosphere varies
2 strongly with time, location and altitude. This makes it necessary to monitor it at both high spatial and
3 high temporal resolution. Mapping the spatial distribution of water vapor in the atmosphere is difficult
4 due to the limited spatial and temporal resolution of contemporary meteorological instrumentation.
5
6
7
8
9

10 It is however also possible to retrieve water vapor estimations from different satellite systems, (Hanssen
11 et al., 1999; Seemann et al., 2003). In this paper two systems are considered. At GPS ground stations, the
12 zenith Integrated Water Vapor (IWV) can be derived from the total delay that the GPS signals undergo
13 while traveling from the GPS satellites to the GPS receiver at the ground stations. This derivation results
14 in relative good IWV estimates with a high temporal (e.g. 1 hour) but a low spatial resolution (tens to
15 hundreds kilometers). The MERIS instrument on the Envisat satellite estimates integrated water vapor
16 by observing the backscatter of solar radiation in the near infrared over land, sea and above clouds. With
17 a maximum spatial resolution of 300 m, MERIS can observe dynamic structures on scales much smaller
18 than possible before. It's temporal resolution however is restricted to 3 days.
19
20
21
22
23
24
25
26
27
28
29

30 For this article we will compare and combine MERIS and GPS IWV data over North-West Europe from
31 August 13, 2003. The GPS-IWV observations consist of a time series of data from 26 ground stations with
32 in general less than hourly temporal resolution. The MERIS data set from the same day, acquired shortly
33 after 10 UTC, has a spatial resolution of 1.2 [km]. The correlation between the two data sources around
34 the acquisition time of the MERIS image will be determined by comparing a selected number of MERIS
35 pixels to the GPS-IWV estimates. An experimental variance-covariance analysis will be made for both
36 data sets. In the MERIS case this analysis will be only spatial, in the GPS case it will be temporal as
37 well. The two data sets will be combined to produce a time series of combined hourly water vapor maps
38 by means of incorporating individual and cross-covariances into a Cokriging system, (Goovaerts, 1997).
39 Except for the water vapor maps itself, this procedure will result in error maps, displaying the errors as
40 propagated from the individual data error components. These results will give a clear insight in the gain
41 that is expected from combining GPS and MERIS water vapor data.
42
43
44
45
46
47
48
49
50
51
52
53
54
55

56 In Section 2 a short introduction is given to the GPS and MERIS systems and to the algorithms used for
57
58
59
60

1 estimating the IWV contents. In Section 3 it is explained how to obtain the spatial and temporal correlation
2 between the different IWV observations and how to combine the observations for a prediction at a certain
3 time and location. In Section 4 GPS and MERIS observations from August 13, 2003 are compared and
4 combined. The paper finishes with discussion of the results and an outlook on further research in Section
5 5.

14 2 GPS and MERIS IWV data

17 2.1 Integrated Water Vapour

18 Water vapor is the gas phase of water. Gaseous water represents a small but environmentally significant
19 constituent of the atmosphere. Most of it is contained in the boundary layer, the lowest 2[km] of the
20 troposphere. In this article we will consider columnar water vapor values. Such values are expressed in
21 [kg/m²], that is as the mass of the water vapor contents in a column of atmosphere above a horizontal
22 square patch of 1[m] × 1[m] on the Earth's surface.
23
24
25
26
27
28
29
30

31 The change in IWV above a fixed point of the Earth's surface can to some extent be described by
32 Taylor's frozen flow assumption, (Taylor, 1938). This hypothesis states that a random field, in our case the
33 water vapor distribution, as a whole is transported by the mean wind. As wind velocities and directions
34 vary with their height above the Earth's surface, Taylor's assumption is of only limited use for direct
35 assessment of Integrated Water Vapour Values. It is reported, (Elgered et al., 2005), that IWV fields often
36 significantly change while traveling one hour upwind.
37
38
39
40
41
42
43
44

45 Knowledge on water vapor values is not only essential for environmental issues but also for satellite
46 measurements from GPS and (In)SAR: the GPS or SAR signal is delayed by atmospheric water vapor.
47
48
49
50

51 2.2 GPS IWV

52 In GPS data processing, measurements from all satellite signal paths are mapped onto the vertical direction
53 by means of a pre-defined mapping function. In this way the effect of GPS signal propagation delay above
54 a GPS station can be estimated. This effect is called the zenith tropospheric path delay. Only the total
55
56
57
58
59
60

effect can be directly estimated from GPS measurements in this way, although in general it consists of two components. The first, hydrostatic, component reflects the impact of dry air on the propagation of the GPS signal and depends on the surface pressure. The second, wet, component appears due to the presence of water vapor in the lower parts of the atmosphere. Therefore, the zenith total delay (ZTD) can be decomposed into two parts: zenith hydrostatic delay (ZHD) and zenith wet delay (ZWD), that is,

$$ZTD = ZHD + ZWD. \quad (1)$$

ZHD can be computed directly as follows

$$ZHD = \frac{0.0022767 \cdot P}{1 - 0.00266 \cos 2\varphi - 2.8 \cdot 10^{-7} H}, \quad (2)$$

where φ is the ellipsoidal latitude of the GPS station, H the orthometric station height and P the surface pressure. ZWD is then obtained from Equation 1. Zenith wet delay can then be mapped into integrated precipitable water vapor (IWV) by means of the following expression:

$$IWV = \Pi \cdot ZWD, \quad (3)$$

where Π is about 0.15 and depends on the mean temperature of the atmosphere, (Bevis et al., 1994; Klein Baltink et al., 2002).

GPS IWV processing. ZTD is estimated along with many other parameters, such as station coordinates, etc., by GPS software suites like the Bernese GPS software, (Rothacher et al., 1996) and OASIS/GIPSY, (Webb and Zumberge, 1993). This process can be performed both in near real-time and in post-processing mode with time resolutions down to 5-6 min. Numerous validation experiments showed that an accuracy of 1-2 kg/m² IWV is achievable for both post-processed and near real-time GPS IWV estimates, (Jarlemark et al., 2002; Klein Baltink et al., 2002; Elgered et al., 2005). The possibility to use data from GPS networks

1 for operational meteorology has been demonstrated in the framework of the COST-716 action (Elgered
2 et al., 2005), which took place in 2001-2004. In 2003, the period under consideration in this paper, ten
3 European Analysis Centers were participating in that action, which involved processing a network of more
4 than 350 stations covering the whole of Europe.
5
6
7
8

9
10
11 **GPS footprint.** The IWV at a given GPS station at a given time is determined from a number of dif-
12 ferent signal paths, one for every visible GPS satellite. If the GPS-IWV estimate is compared to MERIS
13 measurements of 300[m] or 1[km] spatial resolution, an obvious question is what to take for the footprint
14 size and shape of the GPS-IWV estimate. As the configuration of GPS satellites is continuously changing
15 it is at first approach only possible to use an approximate footprint. We assume that the footprint is
16 circular, which is in general not correct, because of gaps in GPS satellite coverage towards the North of
17 GPS ground stations in the Northern hemisphere and towards the South in the Southern hemisphere. The
18 area with no GPS satellites visible in the sky is larger at higher latitudes. Instead of using a fully geometric
19 approach depending on elevation cutoff and signal path geometries, we obtain an optimal radius R_{GPS} as
20 follows. First an upper bound $R_U = 10 / \arctan 10 \approx 15$ [km] for the radius is determined by combining the
21 elevation cutoff angle of 10 degrees with an approximate height of the troposphere, where most water vapor
22 is concentrated, of 10 [km]. Let R vary between 0 and the upper bound R_U of 15[km] and determine in
23 steps of 250 [m] the correlation coefficient between the GPS-IWV estimates and the MERIS-IWV pixels
24 within distance R of the GPS stations. That value of R that gives the highest correlation is chosen as the
25 footprint radius R_{GPS} .
26
27
28
29
30
31
32
33
34
35
36
37
38
39
40
41
42
43
44
45
46
47

48 2.3 MERIS IWV

49 Since its launch on board the Envisat satellite in March 2002, the Medium Resolution Imaging Spec-
50 trometer MERIS gives insight into the properties and dynamics of the Earth system with unprecedented
51 accuracy and resolution. MERIS is a push-broom imaging spectrometer with a spatial resolution of 300m.
52 It measures the solar radiation reflected by the Earth in 15 spectral bands, programmable in width and
53 position, in the visible and near infra-red. The main mission of MERIS is oceanography, observing sea-
54
55
56
57
58
59
60

1 color. The secondary mission of MERIS is to observe, amongst others, the water vapor column over land,
2 water or above clouds. Observations are limited to the day-side. Global coverage is obtained after 3 days.
3
4
5
6
7
8
9
10
11
12
13
14
15
16
17
18
19
20
21
22
23
24
25
26
27
28
29
30
31
32
33
34
35
36
37
38
39
40
41
42
43
44
45
46
47
48
49
50
51
52
53
54
55
56
57
58
59
60

MERIS also retrieves cloud type and top height.

Integrated Water Vapour values are obtained by a differential absorption method from the radiances L_{14} and L_{15} measured in channels 14 and 15, resp., (Bennartz and Fischer, 2001). These channels are centered around 885 and 900 [nm], with a half width value of ± 10 [nm]. The ESA algorithm to derive the IWV estimates, W , is based on the logarithmic relation

$$W = k_0 + k_1 \log \frac{L_{15}}{L_{14}} + k_2 \log^2 \frac{L_{15}}{L_{14}}, \quad (4)$$

between the columnar water vapor and the ratio of the spectral radiances from bands 15 and 14. The k_0 , k_1 and k_2 are regression constants.

The values of the regression constants depend on the viewing geometry. But, there are also differences in methodology for IWV estimates above land and water, (Fischer and Bennartz, 1997). The absorption of water is higher, therefore the aerosol scattering gains influence and is taken into account over water by including the values for the 'aerosol' channels 9, 12, and 13 in the determination of the regression constants. The theoretical accuracy of the estimated water vapor column is 1.7 [kg/m²] over land and 2.6 [kg/m²] over water at full resolution, (Bennartz and Fischer, 2001). The specified accuracy for the IWV contents at the reduced resolution of 1.2 km is specified by ESA as smaller than 20%.

3 Integrating GPS and MERIS data.

Spatial and temporal continuity. Correlation in time or in space between observations can be detected and modeled by a variogram or covariance analysis, (Goovaerts, 1997). The resulting model is used to determine the variance-covariance matrices of the observations. Using the VC-matrices, a Best Linear Unbiased Prediction can be obtained for the IWV content at a given time and location. The underlying assumption used in this framework is that the signal, in our case the IWV, can be considered a random

1 function. This means that every observation is one single outcome of a complete distribution of possible
2 observations at that time and location. Stationarity of a random function means that the expectation of
3 the function value is independent of location or time.
4
5
6

7 The theoretical covariance function of a stationary random function $Z(x)$ is an expectation, E , and is
8 defined as
9

$$10 \text{cov}(s) = E((Z(x) - m)(Z(x + s) - m)), \quad (5)$$

11
12
13
14
15
16
17
18 where $m = E(Z(x))$ denotes the mean of $Z(x)$ and s a temporal or spatial distance. Given a set of
19 observations, a discrete experimental covariance function can be determined by computing experimental
20 covariances between any two observations and by grouping the outcomes according to some distance
21 interval. By fitting the experimental values into a positive definite model, a continuous covariance function
22 is obtained that is used to fill the VC-matrix for a prediction at arbitrary location or moment.
23
24
25
26
27
28
29

30
31
32 **Ordinary Kriging's clustering and screening properties.** Incorporating the variance-covariance structure
33 of the observations into the interpolation method has some important consequences, (Wackernagel, 2003;
34 Chilès and Delfiner, 1999). Two interpolation effects occur that do not occur in case of e.g. inverse distance
35 interpolation. The first effect is known as *clustering*. According to the spatial (or temporal) continuity
36 assumption, close by observations will be highly correlated. This implies that the additional weight obtained
37 by an extra observation in the direct neighborhood of an existing observation will be limited, as according
38 to the high correlation, there is limited new information in the extra observation. This effect is called
39 clustering because weights can be at first instance being thought of as being divided between the different
40 clusters of observations rather than between individual observations.
41
42
43
44
45
46
47
48
49
50

51
52 The second effect is known as *screening* and can be thought of as happening within one cluster. If one
53 observation is behind an other observation with respect to the prediction location, the observation behind
54 contains limited new information. Therefore it will obtain a low weight compared to the observation in
55 front, that is preferred because it is closer to the prediction location. It is even possible that the observation
56
57
58
59
60

behind gets a negative weight. The stress on the weights can be relieved by increasing the so-called *nugget value* or white noise. This value encodes the short time variability or the size of the measurements errors. The clustering and screening effect will have relevant influence on the result, especially for the GPS-IWV observations where the observations are spatially sparse and not regularly spaced.

Spatial-temporal interpolation. The MERIS IWV observations have a high spatial resolution, but only one epoch of observations is available. On the other hand, the GPS IWV observations are spatially sparse but are available at more or less regular time intervals. Therefore it is decided to estimate an IWV value $\hat{I}(t, (x, y))$ at moment t and location $p = (x, y)$ as a linear combination

$$\hat{I}(t, p) = (w_1 \cdot I_{G,1}(p_1, t) + \dots + w_n \cdot I_{G,n}(p_n, t)) + v \cdot I_M(p, t_M) \quad (6)$$

of GPS-IWV observations $I_{G,1}(p_1, t), \dots, I_{G,n}(p_n, t)$ made at n different locations at moment t , and of the (only) one MERIS-IWV observation $I_M(p, t_M)$ at location p , obtained at MERIS-IWV observation time t_M . The weights w_1, \dots, w_n for the n GPS-IWV observations and v for the one MERIS-IWV observation are obtained by solving the following Ordinary Kriging like system.

$$\begin{pmatrix} 1 & cs_{12} & \dots & cs_{1n} & 0 & 1 \\ cs_{21} & 1 & \dots & cs_{2n} & 0 & 1 \\ \vdots & \vdots & \ddots & \vdots & \vdots & \vdots \\ cs_{n1} & cs_{n2} & \dots & 1 & 0 & 1 \\ 0 & 0 & \dots & 0 & 1 & 1 \\ 1 & 1 & \dots & 1 & 1 & 0 \end{pmatrix} \cdot \begin{pmatrix} w_1 \\ w_2 \\ \vdots \\ w_n \\ v \\ \lambda \end{pmatrix} = \begin{pmatrix} cs_{01} \\ cs_{02} \\ \vdots \\ cs_{0n} \\ ct_{0M} \\ 1 \end{pmatrix} \quad (7)$$

The VC-matrix on the left in Equation 7 contains the spatial correlations cs_{ij} between the IWV-GPS observations in the $n \times n$ top left part. The $n + 1$ -th row and column express that no correlation is assumed between the spatial and temporal contributions to the system, while the last row and column

are added for obtaining an unbiased prediction. In the proximity vector on the right, the first n entries contain the spatial correlations cs_{0i} between the prediction location and the locations of the GPS-IWV observations. The $(n + 1)$ -th entry ct_{0M} gives the temporal correlation between the prediction time, t_0 , and the MERIS-IWV observation time, t_M , while the last entry again is obtained from the unbiasedness condition $w_1 + \dots + w_n + v = 1$. Solving System 7 gives a unique solution for the weights, because of the positive definiteness of the VC-matrix.

Except for a IWV prediction $\hat{I}(t, p)$ we obtain a quality description in the form of a (scaled) residual variance $\text{var}_S(r_0)$, with $r_0 = \hat{I}_0 - I_0$ the difference between the prediction \hat{I}_0 and the (unknown) real value I_0 at the prediction space-time point indicated by zero, compare (Goovaerts, 1997; Wackernagel, 2003). The residual variance is given by

$$\text{var}_S(r_0)_{(t,p)} = 1 - \sum_{i=1}^n w_i \cdot cs_{0i} - v \cdot ct_{0M} - \lambda \quad (8)$$

Basically, the residual variance expresses the proximity, both in space and time, to the observations. It is locally minimal at the GPS-IWV observation locations and at MERIS observation time while it increases together with the decrease in correlation between the prediction space-time point and the observations.

This approach is known as the collocated approach. It is fast as the Kriging System 7 is small. The size depends only on the number of GPS ground stations. Moreover the VC-matrix is fixed during the interpolation, which implies that it only needs to be inverted once. The values in the proximity vector however are different for each prediction space-time point. Disadvantage of this method is that it will not fill any spatial gaps in the MERIS grid. This could be resolved for by including a spatial interpolation component for the MERIS observations as well, but then the computational efficiency will be lost.

4 Data description, comparison and combination.

The position of all data considered here is given in WGS84 (World Geodetic System 1984) coordinates, that is, the position of a data point is given by a latitude and a longitude with respect to the WGS84 reference

1 ellipsoid. Distances between points are spheroidal and are computed along (approximate) great circles with
2 respect to this ellipsoid. Time is given in Coordinated Universal Time (UTC), which corresponds to the
3 time zone of Greenwich on the western part of the scene considered.
4
5
6
7
8
9

10 4.1 *GPS data.*

11 The GPS data we used is originating from the 26 GPS COST-716 ground stations, (Elgered et al., 2005),
12 as shown in Fig. 1. We used as much data as possible from one processing center, therefore 24 stations
13 were taken from the GeoForschungsZentrum (GFZ) in Potsdam. Two additional stations processed by
14 the Nordic Geodetic Commission (NKG), were added to improve the spatial coverage. For the given list
15 of stations we consider all available IWV data from August 9, 2003. For the GFZ stations mostly IWV
16 estimates are available at quarter past and quarter before the whole hour, but some data are missing.
17 NKG data is available at 15 minutes interval, but here data points are missing as well.
18
19
20
21
22
23
24
25
26
27
28
29

30 4.2 *Processing the MERIS data.*

31 We used one MERIS reduced resolution product, acquired at August 9, 2003, between 10:11:27 and 10:14:44
32 UTC. At reduced resolution, one pixel is available for every $1.2 \times 1.2 \text{ km}^2$ at nadir direction.
33
34
35
36
37
38

39 **Data flags.** A MERIS Level 2 data set contains an *Integrated Water Vapor* attribute. The value of this
40 attribute at a given position may not always be representing the actual IWV value, due to e.g. the presence
41 of cloud cover. Therefore a filter step is necessary. Except for several data attributes, the MERIS Level 2
42 product also provides a quality attribute by assigning binary 24-bit flags to each product pixel. A unique
43 combination of zeroes and ones addresses the pixel state and quality, according to the classification of the
44 MERIS pixels.
45
46
47
48
49
50

51 We removed IWV points for which the CLOUD flag, the PCD_14 flag, or the TOAVLCSI flag is true,
52 see Fig. 2. The CLOUD flag indicates that a cloud product is available; the PCD_14 flag indicates that the
53 total water vapor content is uncertain while the TOAVLCSI flag indicates Cloud, Snow or Ice over land
54 pixels, according to MGVI processing. For our test data set this filter step reduces the number of points
55
56
57
58
59
60

1 in the scene from 1 256 641 to 1 090 222 points. The other flags were ignored. At the moment it is not
2
3 clear if this is the best way of filtering.
4
5
6
7

8 **4.3 Comparison at MERIS time.**

9

10
11 **Single pixel comparison.** After removal of suspicious MERIS points, a comparison was made between
12 the GPS IWV values at MERIS acquisition time and the values of the remaining MERIS pixels close to
13 the GPS stations. First the MERIS pixel closest to each of the GPS stations was determined, see Fig.
14
15 3. The correlation between these GPS and MERIS estimates is only 0.627. This bad correlation value
16 is mainly caused by some strong outliers. Especially near Stavanger (STAS), Oberpfaffenhofen (OBE2),
17 Pfaender (PFAN) and, to a lesser degree, near Braunschweig (PTBB) and Helgoland (HELG), agreement
18 in estimates is small. Therefore the MERIS pixels around these GPS stations were considered in detail.
19
20
21
22
23
24
25
26
27
28
29

30 **Local situation around GPS stations.** In Fig. 4 the values of 25 MERIS pixels are shown around four
31 GPS stations with values deviating from the nearby MERIS pixel values. The situation around GPS station
32 OBE2 is not considered, as the nearest MERIS pixel after the filtering step of above is already at 10.9
33 [km] distance. Around three stations we observe big jumps between neighboring MERIS pixels: in all three
34 cases jumps of more than 5 [kg/m²] exist. Around STAS even a jump can be found from 25.8 [kg/m²] to
35 49.8 [kg/m²]. An explanation for these jumps can be found in the MERIS flags.
36
37
38
39
40
41
42

43 Near the PTBB station two single flags, 'LAND' and 'PCD_19', are true for all pixels and those pixels
44 all have similar values. Around HELG we see more variability in the MERIS pixel values, and in the flags
45 as well. In this case however pixels with similar values not necessarily have identical flags. What should
46 be noted in this case that all pixels are marked as 'water', so the existence of the two small islands of in
47 total 1.7 [km²] that form Helgoland cannot be recognized on the MERIS image.
48
49
50
51
52
53

54 Around PFAN we find both 'LAND' and 'WATER' pixels. All MERIS pixels with relative high values
55 are 'LAND' pixels. Intermediate values are found at 'LAND' pixels that are marked as 'COASTLINE'
56 pixels as well. Around STAS the situation is the other way around. Here the 'WATER' pixels have high
57
58
59
60

values compared to the 'LAND' pixels. Both in the PFAN and the STAS case however the values of the 'LAND' pixels are nearest to the IWV value as determined by the nearby GPS station.

Correlation MERIS-GPS vs. GPS footprint size. After determining correlation for different footprint sizes of the GPS estimates, as described in Section 2.2, it was found that maximal correlation occurs for $R_{\text{GPS}} = 1.75$ [km]. For this footprint of about 10 km^2 the GPS-MERIS correlation equals 0.79. Using this radius implies that the about 8 MERIS pixels closest to a GPS station were used in the correlation comparison. Note that indeed a maximum in correlation was found inside the interval between 0 [km] and the upper bound of $R_U = 15$ [km], as derived in Section 2.2.

A correlation of 0.853 is obtained if stations are disregarded with a maximal difference of more than 5 kg/[m²] between the MERIS pixels within the GPS footprint. In this way the stations of ONSA, PFAN, STAS and TERS (all coastal!) are removed from the comparison because of big jumps, while DELF and OBE2 have no MERIS data to compare within the GPS footprint.

4.4 Data correlation.

GPS spatial correlation As the number of different GPS station considered is only 26, it is difficult to determine a reliable covariogram for the spatial correlation at a single epoch. Therefore a spatial experimental covariogram is determined from the, if necessary, linearly interpolated GPS measurements at every hour between 0.30 and 23.30. These epoch times are chosen because for most GPS stations and most epochs, IWV estimates are available at exactly the half hours. The covariogram for 10:30 is shown in dark blue in Fig. 5, left. Only those interpolated GPS IWV values were used for the hourly covariograms for which at least one measurement is available within one hour of the covariogram time. The mean of the experimental covariograms obtained in this way is shown in red in Fig. 5, left. This covariogram displays a range, i.e. the maximal distance at which correlation exists, of about 200km and this approximately holds for all individual covariograms as well. The sill, or more precise, the average experimental covariance within the first bin of 60km of the individual covariograms however is highly variable during the day, and varies from

1 40 at 00:30 downwards to -10 at 06:30 and then again upwards via 50 at 10:30 (figure) up to 90 at 15:30,
2
3 in order to end at 23:30 at a value of 65. This shows that the size of the spatial covariance of the IWV
4
5 signal as measured by GPS is highly variable with time although it's range seems more stable. A more
6
7 elaborated approach can be found in (de Haan et al., 2005).
8
9

10
11 **MERIS spatial correlation** The experimental covariogram of a subset of about 1100 MERIS IWV obser-
12
13 vations is represented by the dotted line in Fig. 5, left. Here a bit smaller bin width of 10km is used. This
14
15 covariogram is fairly comparable to the covariogram of the GPS IWV data of 10:30. Due to the higher
16
17 spatial resolution, the range of the MERIS covariogram is higher than the GPS range and is equal to
18
19 almost 500km.
20
21

22
23
24
25 **GPS temporal correlation** The time series of the GPS IWV at the different GPS ground stations display
26
27 a strong trend. Therefore a linear trend was fitted at each station and removed from the data. The mean
28
29 of the 26 temporal covariance functions, determined from the detrended data is given by the brown dots
30
31 in Fig. 5, middle left. As the IWV values at most stations even show some non-linear trend during the
32
33 day, the stationarity condition for the random function does not hold very well. This is expressed by the
34
35 negative covariance values at higher distance.
36
37

38
39
40
41 **Optimizing the GPS IWV prediction.** When producing IWV maps from the GPS IWV observations, the
42
43 additional MERIS observations can be used in two different ways. First of all, the MERIS observations
44
45 are directly incorporated in producing the maps by means of the Cokriging approach. For this purpose
46
47 the individual VC-matrices of both the GPS and the MERIS observations are needed together with the
48
49 cross-correlation VC-matrix containing the cross-covariances between the MERIS and GPS observations.
50

51
52 Moreover, the MERIS IWV observations can be used to gauge and control the covariance parameters of
53
54 the GPS IWV observations. For this purpose the MERIS observations are gridded to a 0.25×0.1 degree
55
56 longitude-latitude grid. This implies that one grid cell has an approximate size of 17×11 [km]. The cell size
57
58 is chosen such that local variations in the MERIS signal are still representable, while the size is not so small
59
60

that computations become too time consuming. The gridding is done by identifying the nearest neighbor in each of the eight octants around a grid-point and combining these eight points to an interpolated value by means of a quadratic inverse distance scheme. Note that in comparison to Fig. 1 all smaller gaps have been filled. Grid points for which no observation is available in all eight octants within 100 km did not get a value.

In the following, this gridded MERIS data set is used as reference data for determining optimal parameters for the interpolation of the GPS-IWV data near MERIS time. As a reference, the mean absolute difference between the gridded MERIS data and the mean of the GPS-IWV observations equals 4.565 [kg/m²]. Two methods were used for interpolation of the GPS-IWV data. For both methods optimal parameter values were determined by minimizing the mean absolute difference at the 0.25 × 0.1 degree longitude-latitude grid between the interpolated MERIS-IWV values and the interpolated GPS-IWV values. Firstly, the GPS-IWV data were interpolated using plain inverse distance, that is every observation gets a weight

$$w_j(p) = \frac{1}{\sum_{i=1}^n (1/d_i^p)} \cdot \frac{1}{d_j^p}, \quad (9)$$

where n denotes the number of observations and d_j the spheroidal distance between the interpolation location and the observation location. Here the only parameter to determine is the power p of the interpolation. The best result, for $p \in \{2, 3, \dots, 6\}$ is obtained for $p = 3$, when the mean absolute difference equals 4.059. The mean absolute difference was determined for different parameters within the ordinary Kriging framework. Here a minimum absolute difference of 3.989 was obtained with a nugget of zero, a sill of 10, and a long range of 3000 [km], while using the exponential model. The result of this interpolation is shown in Fig. 6, middle left. while, at the bottom right, the difference between the interpolated MERIS data and this GPS map is given.

It is remarkable that the experimental covariance functions as derived above indicate a much shorter range of 200 [km] from just the GPS-IWV data and still only 500 [km] from the MERIS-IWV data than

1 found by the optimization procedure of above. Indeed, a range of 500 [km], together with a sill of 50 and
2
3 a filtered nugget of 1, while still using the exponential model, results in a mean absolute difference of
4
5 4.097. The need for using a long range is caused by the often large distances between the interpolation
6
7 locations and the observations. When using a short range, the Ordinary Kriging system will not attach
8
9 higher weights to the nearest observations, as according to the range there is no correlation between the
10
11 prediction location and the observations. As a result, the prediction value will be close to the Kriged
12
13 mean, that is the mean which incorporates the correlation/clustering of the observations. Using a long
14
15 range forces the Kriging system to attend more weight to the nearest observation and this leads to better
16
17 results in comparison to the MERIS data.
18
19

20
21 In Figure 5, right, a difference plot is given between the optimal map as obtained by Ordinary Kriging
22
23 (OK) and by Inverse Distance. For blue points Inverse Distance gives a higher prediction, for red Ordinary
24
25 Kriging is higher. The differences are mostly explainable by the clustering and screening properties of OK
26
27 as discussed in Section 3. In the middle of the picture for example OK gives a higher prediction value. This
28
29 is because the lower observation values in the west of The Netherlands and in Belgium are screened of by
30
31 the higher values at EUSK and WSRA. In the difference picture, Figure 6, right, green indicates under
32
33 estimation by the GPS interpolation and red over estimation. This figure shows that even the (higher)
34
35 OK interpolated GPS-IWV values underestimate the MERIS observations, which shows that in this case
36
37 the OK estimates are closer to the MERIS values as the Inverse Distance estimates. We conclude that for
38
39 interpolation of the GPS IWV stations OK gives the best result. As the number of stations is limited, using
40
41 OK is also feasible from a computational point of view: the variance-covariance matrix of the pair-wise
42
43 correlations between the observations that has to be inverted is small.
44
45
46
47
48
49
50

51 **4.5 *Spatial-temporal combination.***

52
53 In Figure 7, some results of the spatial-temporal interpolation procedure as described in Section 3 are
54
55 shown. The left most figure gives the prediction at 10:30, close to MERIS-IWV observation time. Here
56
57 a lot of small-scale detail is visible, in the same pattern as in Figure 1, that showed the MERIS-IWV
58
59
60

1 observation alone. The combination with the GPS-IWV observations reduces the size of local deviations
2 that are only present in the MERIS-IWV observations however. The middle figure gives a prediction
3 for 14:30 and here the GPS-IWV observations are dominating, but still some smaller scale details are
4 visible, for example off the Norway coast, that were only present in the MERIS-IWV data set. At 18:30 the
5 prediction map is very smooth because it is by now completely dominated by the GPS-IWV observations
6 as there is no temporal correlation anymore with the MERIS acquisition time. The same kind of change in
7 pattern is observed in the prediction map produced for time points before MERIS-IWV acquisition time.

8
9
10
11
12
13
14
15
16
17
18
19
20
21
22
23
24
25
26
27
28
29
30
31
32
33
34
35
36
37
38
39
40
41
42
43
44
45
46
47
48
49
50
51
52
53
54
55
56
57
58
59
60

What remains is to give a good quality description of the IWV predictions obtained in this way. As discussed in Section 3, the Kriging error variance gives an indication for the proximity of the observation points. A step that still has to be added however, is to incorporate the drift of the water vapor field due to wind power into the spatial-temporal interpolation procedure. This step, combined with a validation step using e.g. a one month time series of both GPS-IWV and MERIS-IWV data sets can lead to an adequate quality description of a combined MERIS-GPS water vapor product.

5 Conclusions and further research.

In this paper GPS and MERIS IWV observations are compared and combined.

The MERIS IWV algorithm uses different methods above land and water. This causes large differences between IWV values of neighboring MERIS pixels far beyond the specified accuracy. A further analysis of near-coastal IWV values may lead to an improvement of the current algorithms as used by MERIS for processing IWV data.

For our particular setting we found a correlation of 0.85 when comparing the IWV observation at a GPS station with the average of the MERIS IWV pixels within a circle with optimal radius (GPS footprint) of 1.75 [km]. It should be noted however that stations were removed were a jump of more than 5 [kg/m²] occurred within the GPS footprint. The found correlation value shows that the reported accuracies of the MERIS and GPS IWV observations are consistent.

By determining experimental covariance functions, insight can be gained in the spatial and temporal

1 correlation of the IWV observations. The resulting correlation description can be encoded in a spatial-
2
3 temporal interpolation procedure for combining MERIS-IWV and GPS-IWV observations, similar to Or-
4
5 dinary Kriging.
6

7
8 The spatially dense MERIS-IWV observations can be used as reference data when finding optimal
9
10 parameter values for the spatial interpolation of the GPS-IWV observations. In this way a much longer
11
12 correlation range is found however than by the experimental covariance function analysis.
13

14
15 The results of the spatial-temporal combination of the GPS and MERIS IWV observations match the
16
17 intuition. A next step should be to incorporate wind data in the spatial-temporal combination, as, according
18
19 to Taylor's frozen flow assumption, wind transport water vapor fields as a whole, to some extend.
20

21
22 These first results were obtained with observations of only one day. Testing of larger data sets will allow
23
24 for better validation that should result in an adequate quality description of a final combined MERIS-GPS
25
26 water vapor product.
27

28 29 30 **Acknowledgments.**

31
32 Sybren de Haan from the Dutch Royal Meteorological Society, KNMI is thanked for providing the authors
33
34 with the GPS IWV data and for his useful comments. The MERIS data is distributed by the European
35
36 Space Agency, ESA. This project is funded under number EO-085 by the Netherlands Institute for Space
37
38 Research, SRON.
39
40
41
42

43 44 **References**

- 45
46
47 BENNARTZ, R. AND FISCHER, J. 2001. Retrieval of columnar water vapour over land from back-scattered
48
49 solar radiation using the medium resolution imaging spectrometer (MERIS). *Remote Sensing of*
50
51 *Environment* 78, 271–280.
52
53
54 BEVIS, M., BUSINGER, S., CHISWELL, S., HERRING, T., ANTHES, R., ROCKEN, C., AND WARE, R.
55
56 1994. GPS Meteorology: Mapping Zenith Wet Delays onto Precipitable Water. *Journal of Applied*
57
58 *Meteorology* 33, 379–386.
59
60

- 1 BEVIS, M., BUSINGER, S., HERRING, T., ROCKEN, C., ANTHES, R., AND WARE, R. 1992. Gps mete-
2 orology: remote sensing of atmospheric water vapor using the global positioning system. *Journal of*
3 *Geophysical Research* 97, D14, 15787–15801.
- 4
5
6
7
8 CESS, R. D. 2005. ATMOSPHERIC SCIENCE: Water Vapor Feedback in Climate Models. *Sci-*
9 *ence* 310, 5749, 795–796.
- 10
11
12 CHILÈS, J.-P. AND DELFINER, P. 1999. *Geostatistics: modeling spatial uncertainty*. Wiley Series in
13 Probability and Statistics. John Wiley & Sons, New York.
- 14
15
16 DE HAAN, S., VAN DER MAREL, H., GÜNDLICH, B., AND BARLAG, S. 2005. Resolving spatial and
17 temporal atmospheric water vapour structures using a ground based GPS receiver network. Tech.
18 Rep. project EO-050, SRON.
- 19
20
21
22
23 ELGERED, G., PLAG, H.-P., VAN DER MAREL, H., BARLAG, S., AND NASH, J. 2005. Exploitation
24 of ground-based GPS for operational numerical weather prediction and climate applications, Final
25 report. Tech. rep., COST Action 716, European cooperation in the field of scientific and technical
26 research.
- 27
28
29
30
31
32 FISCHER, J. AND BENNARTZ, R. 1997. Retrieval of total water vapour content from MERIS measurements,
33 algorithm theoretical basis document. Tech. Rep. PO-TN-MEL-GS-0005, ESA-ESTEC, Noordwijk,
34 Netherlands.
- 35
36
37
38
39 GOOVAERTS, P. 1997. *Geostatistics for Natural Resources Evaluation*. Oxford University Press, New York,
40 Oxford.
- 41
42
43 HANSEN, R. F. 2001. *Radar Interferometry*. Kluwer Academic Publishers, Dordrecht.
- 44
45
46 HANSEN, R. F., WECKWERTH, T. M., ZEBKER, H. A., AND KLEES, R. 1999. High-Resolution Water
47 Vapor Mapping from Interferometric Radar Measurements. *Science* 283, 5406, 1297–1299.
- 48
49
50 JARLEMARK, P., JOHANSSON, J., STOEW, B., AND ELGERED, G. 2002. Real time GPS data processing
51 for regional atmospheric delay. *Geophysical Research Letters* 29, 16, 7/1–4.
- 52
53
54
55
56
57
58
59
60 KLEIN BALINK, H., VAN DER MAREL, H., AND VAN DER HOEVEN, A. G. A. 2002. Integrated atmo-
spheric water vapor estimates from a regional GPS network. *Journal of Geophysical Research* 107, D3,

1 4025, doi:10.1029/2000JD000094.

2
3 ROTHACHER, M., BEUTLER, G., BROCKMANN, E., FANKHAUSER, S., GURTNER, W., JOHNSON, J.,
4
5 MERVART, L., SCHAER, S., SPRINGER, T., AND WEBER, R. 1996. The Bernese GPS Software
6
7 Version 4.0. Tech. rep., Astronomical Institute, University of Berne, Switzerland.

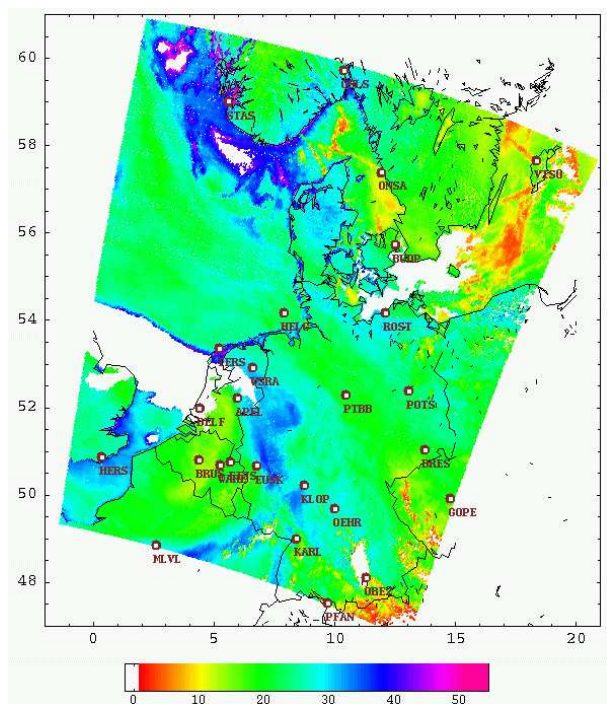
8
9
10 SEEMANN, S. W., LI, J., MENZEL, W. P., AND GUMLEY, L. E. 2003. Operational Retrieval of At-
11
12 mospheric Temperature, Moisture, and Ozone from MODIS Infrared Radiances. *Journal of Applied*
13
14 *Meteorology* 42, 1072–1091.

15
16
17 SODEN, B. J., JACKSON, D. L., RAMASWAMY, V., AND SCHWARZKOPF, M. D. ANDHUANG, X. 2005.
18
19 The Radiative Signature of Upper Tropospheric Moistening. *Science* 310, 5749, 841–844.

20
21 TAYLOR, G. I. 1938. The spectrum of turbulence. *Proceedings Royal Society London, Series A* 164,
22
23 476–490.

24
25
26 WACKERNAGEL, H. 2003. *Multivariate Geostatistics*, Third ed. Springer, Berlin.

27
28 WEBB, F. AND ZUMBERGE, J. 1993. An introduction to GIPSY/OASIS-II. Tech. Rep. D-11088, Jet
29
30 Propulsion Laboratory, Pasadena, California.



GPS Code	Site Name	Proc. center
APEL	Apeldoorn	GFZ
BRUS	Brussel	GFZ
BUDP	Kbenhavn	GFZ
DELF	Delft	GFZ
DRES	Dresden	GFZ
EIJS	Eijsden	GFZ
EUSK	Euskirchen	GFZ
GOPE	Pecny,Ondrejov	GFZ
HELG	Helgoland	GFZ
HERS	Herstmonceux	GFZ
KARL	Karlsruhe	GFZ
KLOP	Kloppenheim	GFZ
MLVL	Marne-La-Vallee	GFZ
OBE2	Oberpfaffenhofen	GFZ
ONSA	Onsala	GFZ
OEHR	Oehr	GFZ
OSLS	Oslo	NKG
PFAN	Pfaender	GFZ
POTS	Potsdam	GFZ
PTBB	Braunschweig	GFZ
ROST	Rostock-Warnemuende	GFZ
STAS	Stavanger	NKG
TERS	Terschelling	GFZ
VIS0	Visby	GFZ
WARE	Waremmme	GFZ
WSRA	Westerbork	GFZ

Figure 1. MERIS water vapor data from August 13, 2003, ± 10:00 o'clock. The MERIS data will be compared and combined with water vapor data from the 26 indicated GPS ground stations.



Figure 2. Classification according to MERIS flags. Clearly visible are the land (white), water (black) and coastline pixels (blue). 'Uncertain total water vapor content' is indicated in red, clouds in light gray and 'cloud, snow or ice over land' pixels are in yellow. These pixels were removed from the MERIS data set.

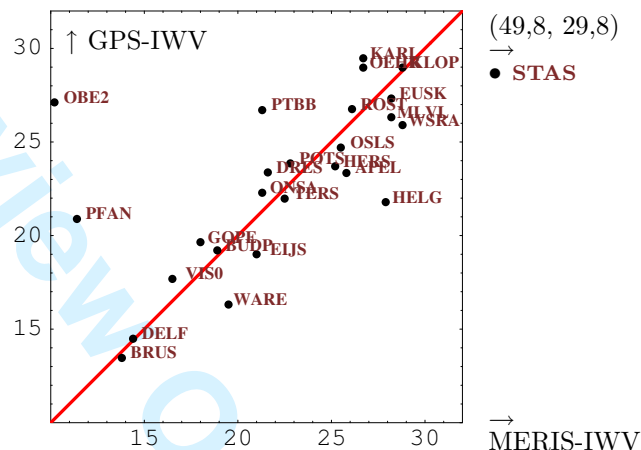


Figure 3. IWV values at GPS stations and at nearest MERIS pixel.

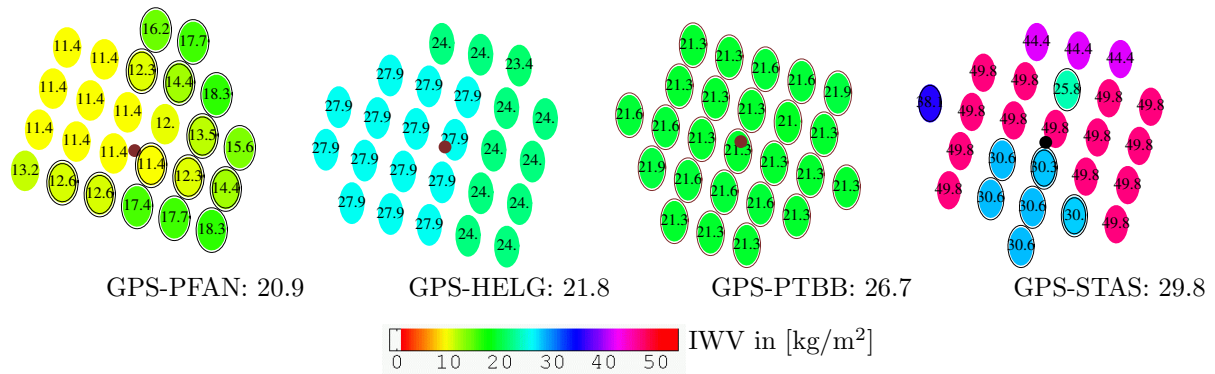


Figure 4. IWV values at 25 MERIS pixels nearest to a GPS station. Top left: Pfaender. Top right: Helgoland. Bottom left: Braunschweig. Bottom right: Stavanger. 'LAND' pixels are surrounded by one circle, 'COASTLINE' pixels by two circles.

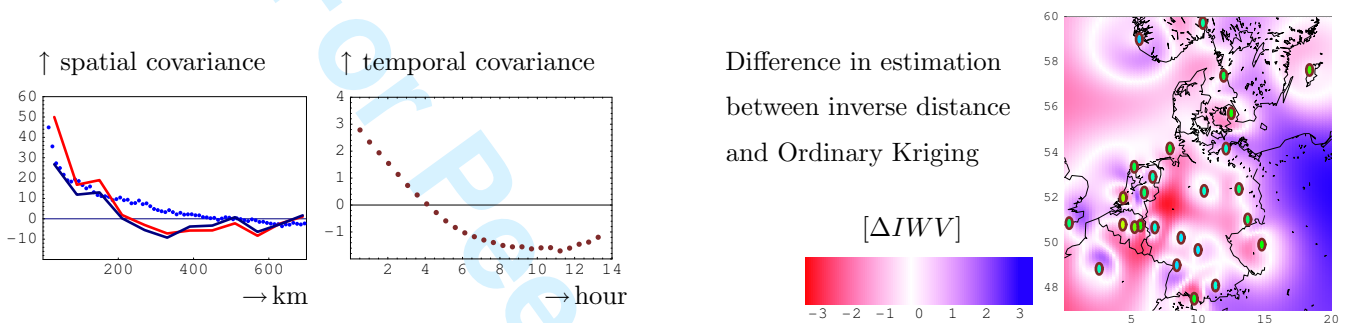


Figure 5. **Left:** Covariograms of the IWV data. Far left: spatial. In dark blue: GPS covariogram at 10:30. In red: mean of 24 hourly spatial GPS covariograms. Dotted: covariogram of the MERIS data. Middle left: temporal. Mean of the 26 temporal covariograms of the detrended IWV values at the different GPS stations. **Right:** difference in interpolated values between optimal inverse distance and Ordinary Kriging approaches.

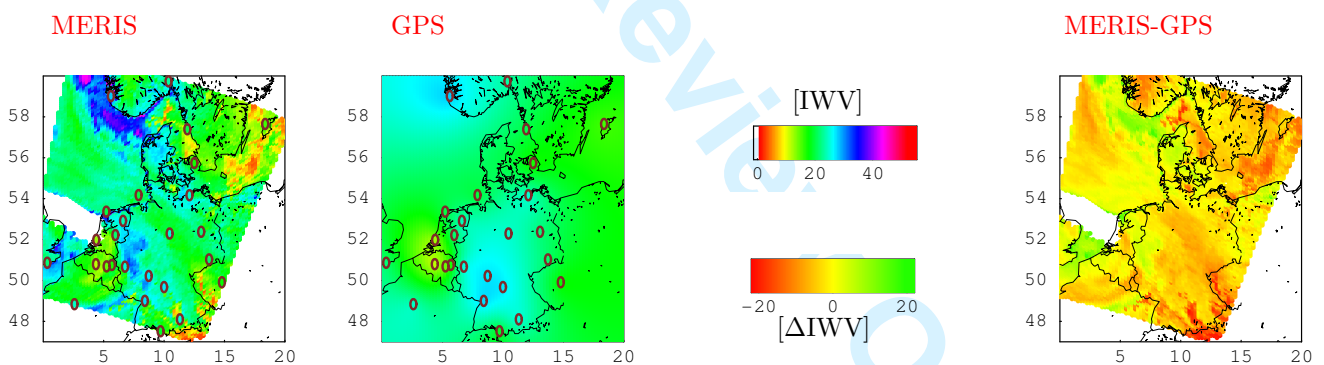


Figure 6. Interpolated MERIS (far-left) and GPS (middle-left) observations at MERIS time. Both data sets are interpolated to the same grid. At the right image the difference between the two maps is given.

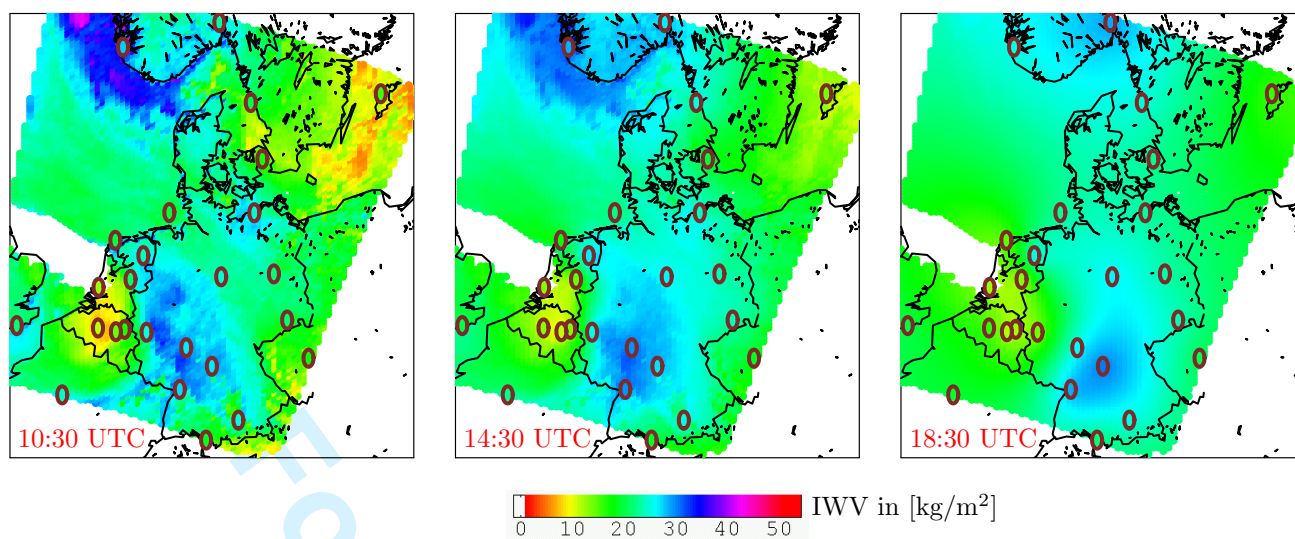


Figure 7. Maps of the IWV contents over North-West Europe at 10:30 UTC, 14:30 UTC and 18:30 UTC, obtained by combining the MERIS-IWV and the GPS-IWV observations.